

Observation of inter-Landau-level quantum coherence in semiconductor quantum wells

K. M. Dani,^{1,2,3} I. A. Cotoros,^{2,3} J. Wang,³ J. Tignon,⁴ D. S. Chemla,^{2,5} E. G. Kavousanaki,^{6,7} and I. E. Perakis⁷

¹ *Materials Science and Technology Division, MST-10,*

Los Alamos National Laboratory, Los Alamos, New Mexico 87545, USA

² *Department of Physics, University of California at Berkeley, Berkeley, California 94720, USA*

³ *Materials Sciences Division, E.O. Lawrence Berkeley National Laboratory, Berkeley, California 94720, USA*

⁴ *Laboratoire Pierre Aigrain, Ecole Normale Supérieure, F-75005 Paris, France.*

⁵ *Materials Sciences Division, E.O. Lawrence Berkeley National Laboratory, Berkeley, California 94720*

⁶ *Chemistry Department, University of California, Irvine, California 92697, USA*

⁷ *Institute of Electronic Structure & Laser, Foundation for Research & Technology-Hellas, and Department of Physics, University of Crete, GR-71003 Heraklion, Greece*

(Dated: June 8, 2018)

Using three-pulse four-wave-mixing femtosecond spectroscopy, we excite a non-radiative coherence between the discrete Landau levels of an undoped quantum well and study its dynamics. We observe quantum beats that reflect the time evolution of the coherence between the two lowest Landau level magnetoexcitons. We interpret our observations using a many-body theory and find that the inter-Landau level coherence decays with a new time constant, substantially longer than the corresponding interband magnetoexciton dephasing times. Our results indicate a new intraband excitation dynamics that cannot be described in terms of uncorrelated interband excitations.

PACS numbers: 78.47.nj, 42.50.Md, 73.20.Mf, 78.67.De

Quantum coherences between discrete states, formed by creating a superposition with well-defined relative phase, are central for manipulating matter on a quantum level and can provide the basis of schemes for information processing. Raman coherences in atomic systems lead to non-linear optical effects with potential technological importance, such as electromagnetically induced transparency and lasing without inversion.¹ For applications, it is desirable to observe and manipulate analogous coherences in semiconductors. Quantum beats due to coherence between heavy and light hole valence band states,² as well as collective excitations in the quantum Hall system³ and spin excitations in quantum dots,⁴ have been reported. Standard two-pulse four-wave-mixing (FWM) experiments do not access directly the Raman coherence, which can be inferred by simultaneously measuring the pump-probe signal⁵ or by using three-pulse wave-mixing.^{3,6} Recently, Spivey *et al.*⁶ demonstrated faster dephasing of the coherence between heavy and light hole excitons than the corresponding interband dephasing.

Here we create and study long-lived coherence between magnetoexcitons in semiconductor quantum wells (QWs), which we control with a perpendicular magnetic (B) field. The QW confinement discretizes the eigenstates along the z -axis (growth direction). The B-field results in quasi-confinement within the x - y plane, thus discretizing the eigenstates into Landau levels (LL). Continuum states are suppressed and the resulting discrete spectrum can be tuned with the B-field. Such effective zero-dimensional confinement opens new possibilities for creating and manipulating coherence. Long-lived intraband coherences could be useful in future applications of quantum technology. Also, understanding the coherence dynamics in QWs subject to a B-field is a necessary step

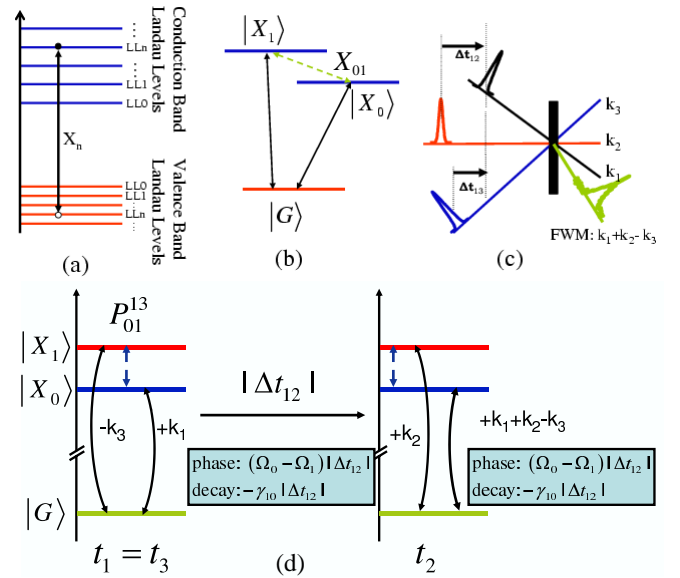


FIG. 1: (Color online) Schematics of (a) X_n states, (b) X_{01} Raman coherence, (c) three-pulse FWM, and (d) nonlinear process describing the X_{01} coherence contribution.

towards a comprehensive picture of the quantum dynamics in the quantum Hall effect regime.^{3,7}

In semiconductors, the Coulomb interaction leads to effects such as exciton-exciton correlations,⁸⁻¹⁰ while exciton coupling to the environment gives both dephasing and new coherences.¹¹ In many-body systems, it is not easy to treat such complex correlations theoretically.⁷ Thus, the measurement of quantities that characterize the coherence dynamics gives valuable information on the non-equilibrium properties of complex systems.

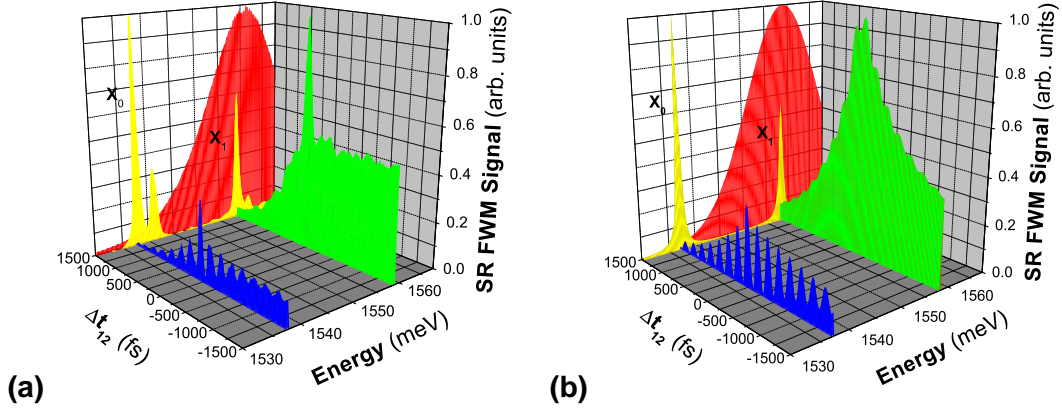


FIG. 2: (Color online) Three-pulse FWM signal along the Δt_{12} axis for large X_1 over X_0 excitation ratio: (a) experiment, and (b) theory. The experimental FWM signals from X_n were obtained using a 1 nm bandwidth interference filter and assigned to the respective linear absorption peaks in this three-dimensional 3D representation. Backplane: Linear absorption and optical pulse intensity.

Here we investigate the dynamics of interaction-induced inter-LL coherence in an undoped QW subject to a large B-field. We photoexcite X_0 and X_1 magnetoexcitons (X_n consists of an electron in the n -th conduction-band LL and a hole in the n -th valence-band LL, Fig. 1a) and create a $X_0 \leftrightarrow X_1$ coherence, X_{01} (Fig. 1b). We identify a three-pulse FWM signal that reflects the dynamics of X_{01} and displays quantum beats with a new decay time. Using a many-body theory,⁷ we identify the source of these beats and extract the dephasing rate of X_{01} . We find that, unlike for uncorrelated magnetoexcitons, this rate is substantially smaller than the sum of the magnetoexciton dephasing rates.

We study a ten well, undoped GaAs QW structure, with 14 nm thick GaAs layers sandwiched between 10 nm thick layers of $\text{Al}_{0.3}\text{Ga}_{0.7}\text{As}$. The sample is kept at 1.5-4°K in a split-coil magneto-optical cryostat. A B-field ($B=0-7$ T) is applied along the QW growth direction. We excite the sample with three 100fs pulses of right-circularly polarized (σ_+) light (Fig. 1c). These pulses propagate along directions \mathbf{k}_1 , \mathbf{k}_2 , and \mathbf{k}_3 , with a time delay Δt_{12} (Δt_{13}) between pulse \mathbf{k}_1 and \mathbf{k}_2 (\mathbf{k}_3). For negative values of the above delays, pulse \mathbf{k}_1 arrives first. We study the transient signal in the background free direction $\mathbf{k}_1 + \mathbf{k}_2 - \mathbf{k}_3$. Using an interference filter, we spectrally resolve this signal and separate the X_0 and X_1 responses. We measure the signal intensity from each state (spectrally resolved FWM) as function of Δt_{12} and Δt_{13} . As explained below, the Δt_{12} axis ($\Delta t_{13} = 0$) accesses the dynamics of the intra-band coherence, while the Δt_{13} axis measures the interband polarization dephasing.

Fig. 1d shows a schematic of the FWM signal due to the X_{01} coherence along the negative Δt_{12} axis. To contribute in the $\mathbf{k}_1 + \mathbf{k}_2 - \mathbf{k}_3$ direction, the inter-LL excitation X_{01} must be created by either \mathbf{k}_1 and \mathbf{k}_3 or \mathbf{k}_2 and

\mathbf{k}_3 pulses. In Fig. 1d, pulses \mathbf{k}_1 and \mathbf{k}_3 arrive together ($\Delta t_{13} = 0$), and create the X_{01} coherence, which evolves for a time $|\Delta t_{12}|$ before it is probed by pulse \mathbf{k}_2 . During this $|\Delta t_{12}|$ time interval, the coherence accumulates a phase at frequency $\Omega_0 - \Omega_1$ and decays with a rate γ_{01} , both reflected in the FWM dependence on Δt_{12} (Ω_n is the energy of X_n). Thus, for $\Delta t_{12} < 0$, we can access the X_{01} coherence dynamics, while, for $\Delta t_{12} > 0$, pulse \mathbf{k}_2 arrives first and the FWM signal reflects the dynamics of

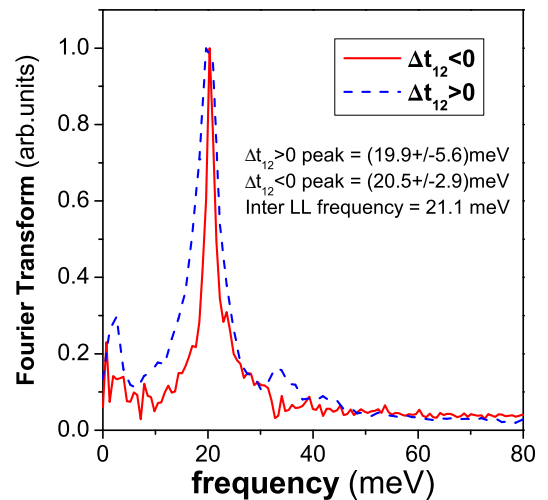


FIG. 3: (Color online) Fourier transform of the oscillations for $\Delta t_{12} < 0$ (solid line) and $\Delta t_{12} > 0$ (dashed line). Both show a single peak at $\Omega_1 - \Omega_0$, but the $\Delta t_{12} < 0$ linewidth (2.9meV) is significantly smaller than the $\Delta t_{12} > 0$ one (5.6meV).

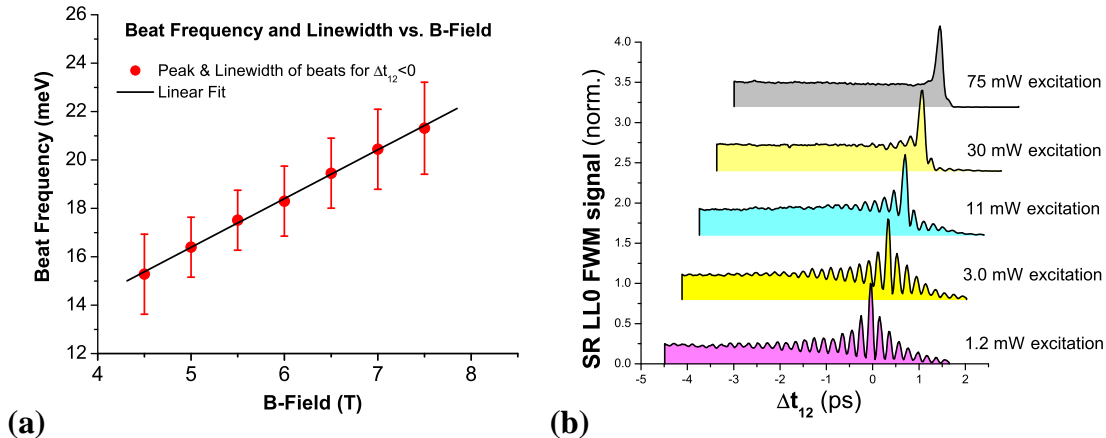


FIG. 4: (Color online) (a) B-field dependence of the oscillation frequency along the Δt_{12} axis. Error bars: linewidths in the oscillation Fourier transforms for $\Delta t_{12} < 0$ (see Fig.3). (b) Intensity dependence of the FWM signal along the Δt_{12} axis. The curves were normalized and shifted for clarity. The x -offset is 0.3 ps, and the y -offset is 0.8.

the interband polarization created by \mathbf{k}_2 .

Fig. 2a shows the FWM intensity from both X_0 and X_1 along the Δt_{12} axis. We largely excite X_1 over X_0 (see backpanel of Fig. 2) in order to suppress the Pauli blocking [phase space filling (PSF)] contribution at X_0 . We then see a very small X_0 signal (as compared to X_1) with striking beats. As discussed above, the negative and positive Δt_{12} axes reflect different dynamics, so we analyze the decay rates separately. We subtract a constant (exponential) background from the negative (positive) axis and take the Fourier transform of the resulting signal (Fig. 3). In both cases, we see a strong peak at energy $\Omega_1 - \Omega_0$, where Ω_1 and Ω_0 are obtained from the linear absorption spectrum (back panel of Fig. 2a). However, we see a large difference in the linewidths obtained by fitting a Lorentzian to the peaks: 2.9 meV for the negative side vs. 5.6 meV for the positive. Therefore, the beats decay slower for $\Delta t_{12} < 0$. This asymmetric decay allows us to identify the X_{01} decoherence time.

Fig. 4a shows the beat frequencies and linewidths extracted from the X_0 FWM signal along the negative Δt_{12} axis for various B-fields. We see a linear dependence of the beat frequency on B, as expected for large B-fields (where the cyclotron energy exceeds the Coulomb energy^{12,13}) from the inter-LL energy $\Omega_1 - \Omega_0$. From the slope of Fig. 4a we extract an e-h reduced mass of $0.058 \pm 0.001 m_e$, which, for electron mass of $0.066 m_e$, corresponds to the heavy-hole mass of $0.498 m_e$. On the other hand, we do not observe any substantial linewidth changes with B. We also studied the changes in the X_0 FWM signal for increasing photoexcitation intensity (Fig. 4b). The decoherence times decrease as the photoexcited carrier density increases, while the asymmetric beat decay and overall temporal profile remain the same.

We analyze our results using a many-body theory⁷ based on the dynamics controlled truncation scheme (DCTS).¹¹ We expand in terms of the optical field in

order to decrease the number of independent dynamical variables and separate out the correlated contributions to the third-order non-linear optical response. We consider σ_+ optical pulses and include for simplicity only the photoexcited X_0 and X_1 states. We use the standard Hamiltonian that treats the Coulomb interactions between carriers in a B-field.⁷ For σ_+ polarized light, the only dipole-allowed optical transition is from the ($j = 3/2, m_j = -3/2$) valence band into the ($1/2, -1/2$) conduction band.¹⁴ This, as well as the measured linear dependence of the beat frequency on the B-field, allows us to consider a simple two band semiconductor model and assume the heavy hole mass of $0.498 m_e$.

The FWM signal from X_n is described by the polarization $P_n = \langle X_n \rangle$. We derive the following equation of motion for P_0 (ignoring the non-resonant terms):

$$i\partial_t P_0 = (\Omega_0 - i\Gamma_0)P_0 + 2\mu E(t)(P_0^L P_0^{L*} + N_0) - 2V_{01}P_0^L (P_1^{L*} P_1^L + N_1) - 2V_{01}P_1^L P_{01} \quad (1)$$

where Ω_0 and Γ_0 are the energy and dephasing rate of X_0 , μ the interband transition matrix element, $E(t)$ the optical pulse, V_{01} the X_0 - X_1 interaction,⁷ P_n^L the linear X_n polarization, $P_{01} = \langle X_{01} \rangle = \langle |X_1\rangle\langle X_0| \rangle - P_0^L P_1^{L*}$ the X_{01} Raman coherence, and N_n the incoherent X_n density. The second term on the right hand side (rhs) of Eq. (1) is due to PSF. The last two terms, due to the Coulomb interaction V_{01} , give a nonlinear coupling of X_0 and X_1 . Setting $N_n = P_{01} = 0$ recovers the semiconductor Bloch equations in a magnetic field.¹² We ignored the bi-magnetoexciton correlations^{7,13} since our FWM signal along the negative Δt_{13} axis, generated by these correlations,^{10,13} is suppressed and decays fast.

The DCTS showed that, in the absence of correlations mediated by a bath, the dynamics can be described in terms of interband amplitudes only.¹¹ It is then impossible to obtain lifetimes longer than the magnetoexciton

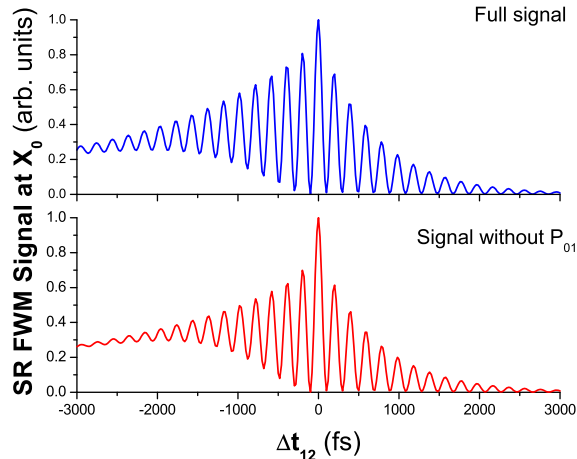


FIG. 5: (Color online) Numerical simulation of the X_0 FWM signal with and without the contribution of the X_{01} coherence.

dephasing times. Here the key variable is P_{01} ,^{7,11}

$$i\partial_t P_{01} = (\Omega_0 - \Omega_1 - i\gamma_{01})P_{01} + i(\Gamma_0 + \Gamma_1 - \gamma_{01})P_0^L P_1^{L*}, \quad (2)$$

which evolves with frequency $\Omega_0 - \Omega_1$ and decays with rate γ_{01} (as in the $|\Delta t_{12}|$ interval of Fig. 1d). The second (source) term is due to the coupling to a bath, characterized by dephasing rates.¹¹ It arises when the X_{01} dephasing rate, γ_{01} , deviates from the sum of the X_n dephasing rates, $\Gamma_0 + \Gamma_1$. In the case of uncorrelated interband transitions, the inter-LL coherence is given by the magnetoexciton amplitude product $P_0^L P_1^{L*}$, which decays with a rate $\Gamma_0 + \Gamma_1$. This Hartree-Fock result gives the third term on the rhs of Eq.(1).¹² $\gamma_{01} \neq \Gamma_0 + \Gamma_1$ implies correlations, mediated by the bath, between the interband transitions. The dynamics of intraband and interband coherences can then be distinguished.

A microscopic calculation of γ_{01} and Γ_n requires complete knowledge of the coupling to the bath. Ref.[7]

analyzed the Coulomb coupling to a cold electron gas. Ref.[11] demonstrated different time evolution of inter-band and intra-band variables due to exciton-phonon dynamics. In our system, dephasing arises from the interplay between phonon-carrier and carrier-carrier scattering and the disorder, which breaks the LL degeneracy, leading to a finite LL width. A complete theory of this interplay is lacking at present. However, our results clearly show different time evolution of X_n and X_{01} due to the bath.

The numerical solution of our full equations, including nonresonant contributions, gives the FWM signal of Fig. 2b. This reproduces the experimental features. The signal due to the term $\propto P_1^L P_{01}$ in Eq.(1) reflects the phase accumulated by P_{01} during $|\Delta t_{12}|$, while the term $\propto P_0^L N_1$ gives $P_0 \propto e^{\gamma_D \Delta t_{12}}$, where γ_D is the relaxation rate of the incoherent X_1 population. We attribute our long-lived coherence to the beating of the two above contributions, with frequency $\Omega_1 - \Omega_0$, which decays at a rate of $\gamma_{01} + \gamma_D \sim \gamma_{01}$. All other FWM contributions lead to oscillations that decay as $\Gamma_0 + \Gamma_1$ or faster. On the other hand, for positive Δt_{12} , all beatings have frequency $\Omega_1 - \Omega_0$ and decay as $\Gamma_0 + \Gamma_1$.¹⁵ This is illustrated in Fig. 5: without the P_{01} contribution, the oscillations for both positive and negative Δt_{12} decay with $\Gamma_0 + \Gamma_1$; however, including P_{01} with $\gamma_{01} < \Gamma_0 + \Gamma_1$, the oscillations decay more slowly on the negative axis. With increasing photoexcited carrier density, carrier-carrier scattering enhances γ_{01} and Γ_n , so the quantum beats decay faster as the intensity increases (Fig. 4b). However, the overall FWM temporal profile remains unchanged, reflecting population relaxation with very small γ_D . We extract from the $\Delta t_{12} < 0$ oscillation decay an inter-LL coherence dephasing rate of $\gamma_{01} = 2.9$ meV. Our work demonstrates tunable quantum dynamics between Coulomb-coupled discrete Landau levels.

This work was supported by the Office of Basic Energy Sciences of the US Department of Energy and by the EU STREP program HYSWITCH.

¹ K. J. Boller, A. Imamoglu and S. E. Harris, Phys. Rev. Lett. **66**, 2593 (1991); A. S. Zibrov, M. D. Lukin, D. E. Nikonov, L. Hollberg, M. O. Scully, V. L. Velichansky, and H. G. Robinson, Phys. Rev. Lett. **75** 1499 (1995).

² M. E. Donovan, A. Shülzgen, J. Lee, P.-A. Blanche, N. Peyghambarian, G. Khitrova, H. M. Gibbs, I. Romyantsev, N. H. Kwong, R. Takayama, Z. S. Yang, and R. Binder, Phys. Rev. Lett. **87**, 237402 (2001); K. B. Ferrio and D. G. Steel, Phys. Rev. Lett. **80**, 786 (1998); M. Joschko, M. Woerner, T. Elsaesser, E. Binder, T. Kuhn, R. Hey, H. Kostial, and K. Ploog, Phys. Rev. Lett. **78**, 737 (1997); T. Dekorsy, A. M. T. Kim, G. C. Cho, S. Hunsche, H. J. Bakker, H. Kurz, S. L. Chuang, and K. Köhler, Phys. Rev. Lett. **77**, 3045 (1996).

³ K. M. Dani, J. Tignon, M. Breit, D. S. Chemla, E. G.

Kavousanaki, and I. E. Perakis, Phys. Rev. Lett. **97**, 057401 (2006); N. A. Fromer, C. E. Lai, D. S. Chemla, I. E. Perakis, D. Driscoll, and A. C. Gossard, Phys. Rev. Lett. **89**, 067401 (2002).

⁴ M. V. Gurudev Dutt, J. Cheng, B. Li, X. Xu, X. Li, P. R. Berman, D. G. Steel, A. S. Bracker, D. Gammon, S. E. Economou, R.-B. Liu, and L. J. Sham, Phys. Rev. Lett. **94**, 227403 (2005).

⁵ S. A. Hawkins, E. J. Gansen, M. J. Stevens, A. L. Smirl, I. Romyantsev, R. Takayama, N. H. Kwong, R. Binder, and D. G. Steel, Phys. Rev. B **68**, 035313 (2003).

⁶ A. G. VanEngen Spivey, C. N. Borca, and S. T. Cundiff, Solid State Commun. **145**, 303 (2008).

⁷ A. T. Karathanos, I. E. Perakis, N. A. Fromer, and D. S. Chemla, Phys. Rev. B **67**, 035316 (2003); I. E. Perakis and

- E. G. Kavousanaki, Chem. Phys. **318**, 118 (2005); K. M. Dani, E. G. Kavousanaki, J. Tignon, D. S. Chemla, and I. E. Perakis, Solid State Commun **140**, 72 (2006).
- ⁸ D. S. Chemla and J. Shah, Nature **411**, 549 (2001).
- ⁹ W. Schäfer and M. Wegener, *Semiconductor Optics and Transport Phenomena* (Springer, Berlin, 2002).
- ¹⁰ P. Kner, S. Bar-Ad, M. V. Marquezini, D. S. Chemla, and W. Schäfer, Phys. Rev. Lett. **78**, 1319 (1997).
- ¹¹ V. M. Axt, K. Victor, and A. Stahl, Phys. Rev. B **53**, 7244 (1996); V. M. Axt and S. Mukamel, Rev. Mod. Phys. **70**, 145 (1998).
- ¹² C. Stafford, S. Schmitt-Rink, and W. Schaefer, Phys. Rev. B **41**, 10000 (1990).
- ¹³ T.V. Shahbazyan, N. Primozich, and I. E. Perakis, Phys. Rev. B **62**, 15925 (2000).
- ¹⁴ N. A. Fromer, C. Schüller, C. W. Lai, D. S. Chemla, I. E. Perakis, D. Driscoll, and A. C. Gossard, Phys. Rev. B **66**, 205314 (2002).
- ¹⁵ When $\Delta t_{12} > 0$ (and $\Delta t_{13} = 0$), pulse \mathbf{k}_2 arrives first. It creates a polarization P_n^L that evolves for time $t = \Delta t_{12}$ with frequency Ω_n and decay rate Γ_n , until pulses \mathbf{k}_1 and \mathbf{k}_3 come in. Different processes can then take place, but the FWM signal emitted in the $\mathbf{k}_1 + \mathbf{k}_2 - \mathbf{k}_3$ direction will only depend on Δt_{12} as $e^{-i\Omega_n \Delta t_{12}} e^{-\Gamma_n \Delta t_{12}}$. Thus, the only oscillations that can be created beat with frequency $\Omega_1 - \Omega_0$ and decay as $\Gamma_0 + \Gamma_1$.